Vis Comput (2009) 25: 873–882
DOI 10.1007/s00371-009-0317-5

ORIGINAL ARTICLE

Motion study of the hip joint in extreme postures

Caecilia Charbonnier · Lazhari Assassi · Pascal Volino · Nadia Magnenat-Thalmann

Published online: 3 March 2009

Abstract Many causes can be at the origin of hip osteoarthritis (e.g., cam/pincer impingements), but the exact pathogenesis for idiopathic osteoarthritis has not yet been clearly delineated. The aim of the present work is to analyze the consequences of repetitive extreme hip motion on the labrum cartilage. Our hypothesis is that extreme movements can induce excessive labral deformations and lead to early arthritis. To verify this hypothesis, an optical motion capture system is used to estimate the kinematics of patient-specific hip joint, while soft tissue artifacts are reduced with an effective correction method. Subsequently, a physical simulation system is used during motion to compute accurate labral deformations and to assess the global pressure of the labrum, as well as any local pressure excess that may be physiologically damageable. Results show that peak contact pressures occur at extreme hip flexion/abduction and that the pressure distribution corresponds with radiologically observed damage zones in the labrum.

Keywords Motion capture · Physically-based simulation · Extreme motion · Hip osteoarthritis

C. Charbonnier (✉) · L. Assassi · P. Volino
MIRALab, University of Geneva, 7, rte de Drize, 1227 Carouge, Switzerland
e-mail: charbonnier@miralab.unige.ch

N. Magnenat-Thalmann
MIRALAB-CUI, University of Geneva, 24 rue Général Dufour, 1211 Genève 4, Switzerland
e-mail: thalmann@miralab.unige.ch

1 Introduction

Osteoarthritis (OA) affects the hip joint and is a common problem for many people. This pathogenesis can be caused by femoroacetabular impingements (FAI) that occur when there is an abnormal contact between the proximal femur and the acetabular rim [19]. Generally, two basic mechanisms of impingement can be distinguished (Fig. 1): the cam FAI caused by a non-spherical femoral head and the pincer FAI due to acetabular overcoverage. These morphological abnormalities induce degenerative lesions of the cartilages and, more specifically, lesions of the superior labrum [43].

Although the mechanism of degeneration in the cam/pincer FAI hip is well understood, the exact pathogenesis for idiopathic OA has not yet been clearly delineated. Indeed, changes in the movement and alignment of the hip (e.g., subluxation) can be other potential causes of early OA. In particular, athletes seem to present a higher risk of developing arthritis due to repetitive and extreme movements performed during their daily exercises [6, 35, 40]. To detect arthrogenous activities, a clinical study with 30 professional ballet dancers is being conducted. The aim of this study is to verify if repetitive extreme motion could be a factor of joint degeneration through excessive labral deformations.

To pursue this goal, an optical motion capture system is used to obtain bone poses of patient-specific hip joint 3D models, reconstructed from magnetic resonance imaging (MRI) data. The major drawback with this system is the soft tissue deformation due to muscle contractions, causing markers movements with respect to the underlying bones. Thus, rigid motion of the bony segments cannot be robustly estimated. To solve this issue, we propose a correction method combining nonlinear optimization and joint motion constraints, and allowing some shifts at the joint. The esti-

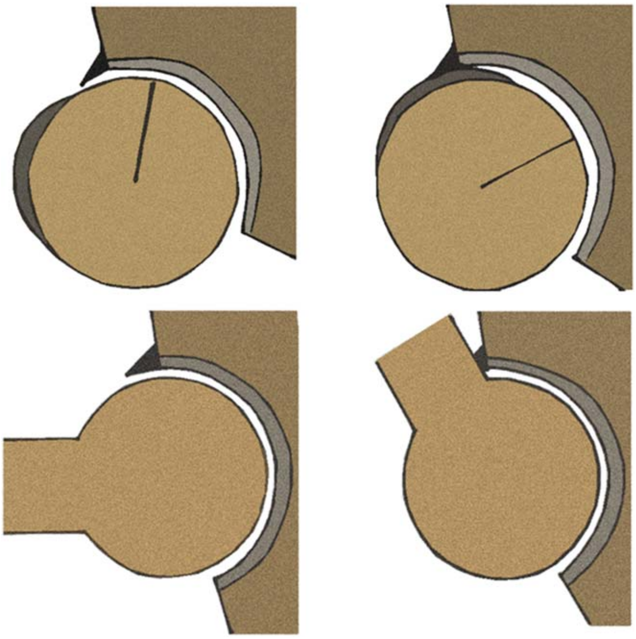

Fig. 1 *Top*: Reduced head-neck offset of cam FAI: non-spherical head abuts the acetabular rim. *Down*: Excessive overcoverage of the femoral head by acetabulum in pincer FAI, causing abutment against the acetabular rim

mation of the hip kinematics was successfully validated with data collected from a dynamic MRI protocol.

Subsequently, a fast functional joint model is used to simulate the mechanical behavior of the soft tissues during motion. To this end, we have developed a physical simulation system that aims at computing accurately the deformations of the cartilage during the joint motion, estimated from the optical capture system. The goal is to compute precisely the strain and stress, in order to assess the global pressure of the labrum, as well as any local pressure excess that may be physiologically damageable.

Finally, simulation results are presented for one dancer and for various extreme dancing movements, and are compared with the radiological analysis of patient's MR images. Moreover, a morphological analysis is performed using standard measurements (e.g., femoral alpha neck angle, acetabular depth and version), typically used to diagnose cam/pincer FAI. Since our hypothesis is that the hip OA is not only the result of cam/pincer FAI, the prevalence of the subject's hip joint must be evaluated, in order to confirm that repetitive extreme motion may lead to labral microtrauma.

2 Related works

To derive the motion of the skeleton, various methods with direct access to the bone (e.g., intra-cortical pins [5, 33], external fixators [11], percutaneous trackers [30, 39], fluoroscopy [20, 50]) have been proposed. These techniques are robust, but they are strongly invasive and impede natural motion patterns. Therefore, the optical motion capture system appears as a non-invasive solution for studying the kinematics of the joint, allowing the recording of a large range of motion. However, the internal bone remains inaccessible and the resulting estimations are embedded with soft tissue artifacts (STA). Displacements of individual markers of more than 20 mm are observed [11] and the STA associated with the thigh is greater than any lower limb segment.

Several methods were proposed to reduce these errors, but these techniques have the following limitations: 1) A recent study [12] has showed that some mathematical approaches [2] are unstable and do not perform better than traditional bone pose estimators (e.g., SVD algorithm [49]). These approaches are thus not efficient to compensate STA; 2) Some methods [9, 37] are based on invalid assumptions (e.g., assuming that the skin motion during a static posture is the same as during the dynamic activities); 3) Some techniques [36] are limited to the use of ball and socket joints (i.e., meaning that no shifts are allowed), which simplifies the joint structures and is not subject-specific.

To overcome this issue, we propose to extend previous works with a correction method combining nonlinear optimization (i.e., we use a quadratic algorithm for robustness and fast convergence) to optimize joint center locations and segment orientations, and joint constraints to avoid non-physiological joint translation and even dislocation due to STA [31]. However, our approach is not meant to impose strong kinematics constraints, as this was addressed in [36]. We rather aim at applying little joint constraints, allowing some shifts at the joint.

Once the femoroacetabular movements are precisely estimated, they provide the motion input for the physically-based simulation. The analysis of the stress and contact distribution in the acetabulum region was the focus of several studies. *In vitro* and *in vivo* measurement methods were developed based on miniature pressure transducers, inserted into the femoral head of cadaveric hips [8, 17] or into implanted prostheses [29]. Unfortunately, these methods are not patient-specific or are invasive and difficult to set up. As a result, mathematical models were implemented to compute non-invasively the mechanics of subject-specific hip joints. They are divided into two categories: analytical and numerical models. Analytical models are based on simple mathematical equations and geometrical parameters [41], whereas numerical models are based on either Mass–Spring [32, 38] systems or Finite-Element methods (FEM) [1, 13, 46]. These latter methods were also used to investigate normal and pathological hip joints (e.g., dysplastic hip [46], cam/pincer FAI hip [13, 14]). However, these studies do not generally simulate complex geometrical 3D meshes (for instance patient-specific models) during sophisticated movements. Indeed, the movement is typically simplified to simple anatomical angles or to low amplitude motion. Therefore, we believe that the combination of physical simulation and motion capture can be an effective approach to study the hip joint in extreme postures.

3 Material and methods

Our study is conducted with professional female ballet dancers. The institutional medical-ethical committee approved the study and the subjects gave written informed consent. For each dancer, patient-specific 3D models (1 femur, 1 hip bone, 1 labrum and 1 skin) of the hip joint were reconstructed from a static MRI protocol [22]. The reconstruction is based on discrete deformable models used to automatically register generic models onto individual static MRI data.

The acetabular region represents the contact area. Since our goal is to assess the labral deformations during extreme movements, only the labrum was tetrahedralized (∼4 K tetrahedra), whereas the 3D models of the bones were hypothesized as rigid bodies. A method based on the medial axis information was used to construct the corresponding tetrahedral mesh, as depicted in [3].

3.1 Motion recordings

Two clusters of six 7 mm spherical markers were affixed onto the lateral and frontal parts of both thighs. Six markers were also stuck on the pelvis (Fig. 2a). These skin markers were arranged to ensure their visibility to the cameras throughout the range of motion. Additional reflective markers were distributed over the body to confer a more complete visualization from general to detailed.

Data from the subjects were acquired during 3 different dancing activities: grand plié, frontal split and developpé à la seconde (Fig. 2b, c, d). These movements have been chosen,

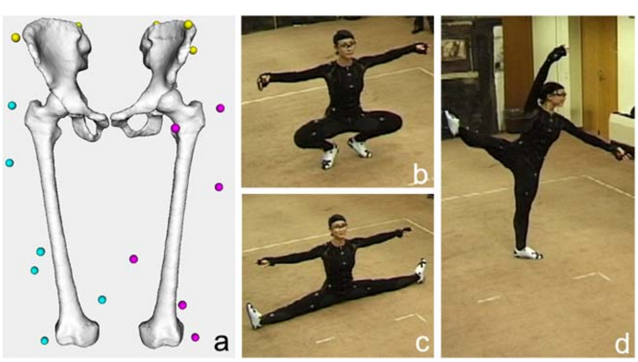

Fig. 2 (**a**) Skin markers configuration: *yellow markers* are fixed to the pelvis, *blue* and *pink markers* are fixed to the right and left thigh, respectively (**b**, **c**, **d**). Dancing movements recorded with the Vicon system: grand plié (**b**), frontal split (**c**) and developpé à la seconde (**d**)

because they require extreme hip flexion and/or abduction. Moreover, they seem to create significant stress in the hip joint, according to some dancer's pain feedback. The markers trajectories were tracked within a 45.3 m^3 measurement volume (3.6 × 4.2 × 3 m) using 8 infrared cameras (Vicon MX 13i, Oxford Metrics, UK), sampling at 120 Hz.

3.2 Anatomical calibration

Before converting markers trajectories into animation, an anatomical calibration is necessary to put in correspondence anatomical and motion frames. This calibration entails the localization of the bone segments in the marker cluster technical frame (CTF) (i.e., the frame determined using marker point coordinates) and the determination of the relevant anatomical frames (AFs) (i.e., the local frames rigidly associated with the bone segments).

In most kinematic studies, bone segment locations and orientations in the CTF are established from a number of calibrated anatomical landmarks (ALs), located by external palpation [10]. Then, through obvious geometric calculations and using the reconstructed positions of the ALs, the relevant AFs are computed. However, this methodology lacks accuracy and precision in the determination of ALs, due to the overlying soft tissues or to AL misplacement [16]. This affects AF position and orientation precision and, consequently, the estimation and interpretation of joint kinematics.

To cope with the inaccuracies in the determination of ALs, we computed the pelvic and femoral coordinate systems from ALs defined directly on the 3D models of the bones. These AFs were implemented following the recommendations of the Standardisation and Terminology Committee of the International Society of Biomechanics [51] to report joint motion in a repeatable way. The same bone models were used to evaluate the hip joint center's (HJC) position using a functional method, detailed in [21].

To establish the correspondence between the markers setup and the bone segments, our idea is to combine MRI and 3D body scan information to have a better approximation due to marker positions on the skin. Indeed, 3D body scanning is a modality that digitalize accurate skin models of the complete body (accuracy ≈1 mm). Following motion recordings, the subjects underwent a 3D body scan (Vitus Pro, Vitronic, Germany) with the markers still in place to retrieve their exact external body surface. From this acquisition, a body contour of the subject is produced and accurately fitted to a generic body model [48]. Moreover, the positions of the skin markers are easily identified on the scan data, using a least-squares sphere fitting technique [47]. Subsequently, a registration method is used to conform the body model and the extracted marker positions to the generic skin segmented from MR images. Since the MRI skin model is limited to the pelvis and the femur, the registration method works in two steps (Fig. 3):

Step 1: The body model surface from the pelvis to the knee is conformed to the MRI skin model through barycentric coordinates, previously stored from a single subject manual registration. The power of using generic shapes is that the morphological features have the same vertex indexes across individual models. Therefore, since the body model and the MRI skin model are both generic, only one single subject manual registration is required to compute the geometric correspondences (i.e., the barycentric coordinates) between the two models. Then, the body model can be easily conformed to the MRI skin model for all other individuals, using those correspondences.

To visually evaluate the registration accuracy, the contours of the two surfaces are drawn on the MRI slices (Fig. 3d). The registration is considered as accurate, when the two contours are perfectly aligned for the entire MRI volume.

Step 2: Rigid registrations are performed for the other body parts (i.e., the two shanks and the torso) using a least-squares minimization. To proceed, the following procedure is performed:

Let us consider a set of points $\{x_i \in \mathbb{R}^3\}_{i=1}^n$ belonging to the body model surface from the pelvis to the knee, at the junction of the torso (Fig. 3e). These points are transformed in Step 1 and their new positions are denoted by $\{y_i \in \mathbb{R}^3\}_{i=1}^n$. We seeks for the best rigid transform Rt that minimize the function:

$$\min \sum_{i=1}^{n} \| Rx_i + t - y_i \|^2 \tag{1}$$

with R the rotation matrix and t the translation vector. The resulting rigid transform is used to register the torso. For the two shanks, the same procedure is applied by selecting appropriate points on the body model surface. Since our focus is on the hip joint, simple approximations for these parts are satisfactory.

Finally, markers which are attached to the body model surface follow the transformation of the body model. As a result, the body model is replaced in the MRI space. A calibration frame is also obtained where the relative position of the skin markers, with respect to the underlying bone, is now established.

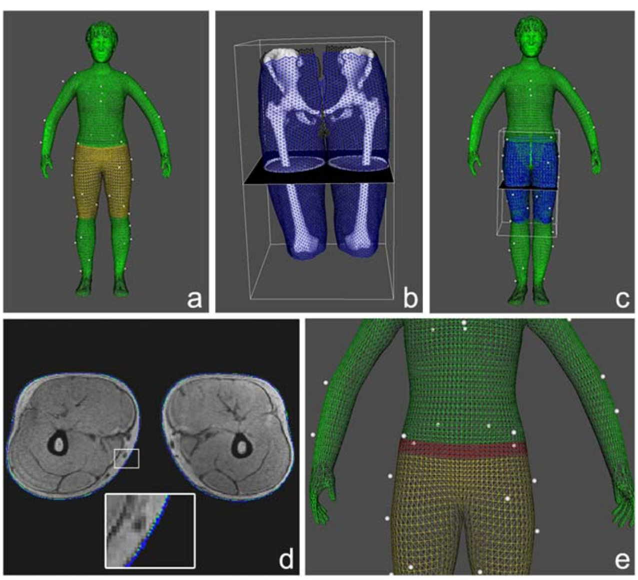

Fig. 3 (**a**) The markers and the body model segmented into 2 parts: the *yellow part* is conformed to the MRI skin model and the *green parts* are rigidly registered. (**b**) The MRI skin model with the reconstructed bones and the MRI volume. (**c**) Registration result (the bones are not shown for clarity). (**d**) The surface contours drawn in one MRI slice. The *green* (body model) and *blue* (MRI skin model) *contours* are perfectly aligned. (**e**) The points at the junction of the torso (*red*) used to compute the rigid transform of the torso

3.3 Bone poses estimation

Rigid motion of the bone segment cannot be robustly estimated from the markers trajectories, unless the STA is small. To reduce STA, our correction method works in 2 phases: 1) First, we combine nonlinear optimization and joint constraints. The optimization provides us for each segment with the rotation and translation that minimize the error made globally on all the markers, while the HJC remains fixed during this first phase; 2) Although the HJC can be considered as fixed during low amplitude movements, this is not true for extreme motion. Indeed, a potential subluxation may occur to avoid bones penetration. Thus, our algorithm adjusts the HJC by detecting collisions among the articulating bones, the goal being to reach the non-penetrating state. More details about these 2 phases are given below:

Phase 1: During a movement, several components contribute to the motion of a skin marker. Assuming that the pelvis motion is known, the HJC can slightly move during the rotation of the thigh. This introduces one translation T_c and one rotation R. Additionally, a rigid displacement is observed due to STA which is denoted by another translation T_s. The motion of a marker with respect to the pelvis can hence be described by 3 transformations successively applied. Since we cannot accurately estimate both T_c and T_s simultaneously, one of the translations must be discarded. Previous works [11] showed that, for the thigh, the magnitude of the STA is greater than the displacement of the joint center. Therefore, we decided to compute the best estimate of T_s and to assume that T_c is close to null. On the contrary, for the pelvis, it appears that the STA remains small. Thus, for this bone we assumed that T_s is close to null and we estimated T_c instead.

In order to find the transformation (3 unknowns for the rotation in an axis-angle form and 3 for the translation) that minimizes the error made globally on the markers, the objective function to minimize for each segment and for each instant frame is as follows:

$$\sum_n (p_i - p_i')^2 \tag{2}$$

with n the number of markers attached to the bone segment, p_i the recorded position of the ith marker, and p_i' its estimated position. This is a least-squares minimization for which we used the rfsq optimizer [34]. Since the skin markers move nonlinearly [11], the solution converges faster thanks to the quadratic programming algorithm.

Phase 2: We assume that the position of the pelvis is correct, because the magnitude of the STA remains small for this bone. In case of collision between the articulating bones, the position of the femur must be hence corrected, for each instant frame, in order to reach the non-penetrating state. This correction corresponds to a translation of the HJC of vector $\mathbf{D}_{\mathrm{HJC}}$ (boldface notation for vector). For fast computation, an uniform-level octree subdivision [24] is used for the hip bone model and the following algorithm is applied (see Fig. 4):

Let us consider Φ being the *collider* (i.e., the femur) and Γ the *collided object* (i.e., the hip bone). The two meshes are defined by a set of points $\Phi = \{P_i \in \mathbb{R}^3\}$ and $\Gamma = \{Q_i \in \mathbb{R}^3\}$, respectively. First, we project each point P_i onto Γ, yielding the projected point $P_{i\perp}$. Then, P_i is defined as being inside, and therefore colliding, if $\mathbf{P}_i\mathbf{P}_{i\perp}.\mathbf{N}_{\mathbf{P}_{i\perp}} > 0$ where $\mathbf{N}_{\mathbf{P}_{i\perp}}$ is the outward normal at $P_{i\perp}$. This subset of k colliding points $C_k = \{P_1, \dots, P_k\}$ creates the displacement vector:

$$\mathbf{D} = \frac{\sum_{i=1}^{k} \mathbf{P}_i\mathbf{P}_{i\perp}}{k} = \frac{\sum_{i=1}^{k} \mathbf{d}_i}{k}. \tag{3}$$

The *collider* undergoes a translation proportional to the vector $\mathbf{D}$. This algorithm is iteratively performed for each instant frame, until no more collisions are detected. As a result, the translation $\mathbf{D}_{\mathbf{HJC}}$ of the HJC is equivalent to the sum of the translation vectors applied on the *collider*.

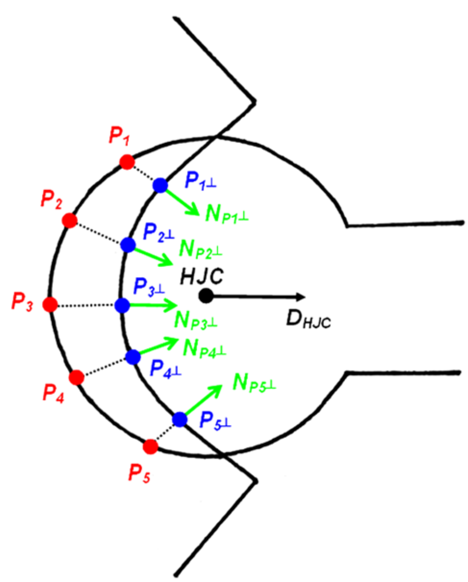

Fig. 4 2D schematic view of the collisions detection algorithm. The femur is corrected at each instant frame. As a result, the HJC undergoes a translation of vector $\mathbf{D}_{\mathrm{HJC}}$

Validation: The validation of the hip kinematics estimation was obtained using marker position data, collected during clinical motion patterns (flexion/extension, abduction/adduction, internal/external rotation) on 6 volunteers scanned with a dynamic MRI protocol [23]. The subjects were equipped with external MRI-compatible marker sets and a tracking device was used to ensure the movements repeatability. For each instant frame, the position and orientation of both the hip and femur bones were computed and the kinematics derived from the marker position data were compared with that of the MRI bone tracking. Only the error on the femur translation/orientation was calculated, since no markers were placed on the pelvis. Table 1 shows the femur position and orientation reconstruction errors expressed in the hip joint coordinates system.

As said previously in Sect. 2, the femur exhibits substantial skin motion. From these results, the STA errors for this bone are thus significantly reduced by the use of the proposed method.

3.4 The simulation model

The base of this simulation model is a first-order finite-element system [4, 7, 15], which offers a good tradeoff between accuracy and computation speed in the context of soft tissues. Since the only degrees of freedom of such models are the vertices of the mesh, it can be associated to any fast numerical integration method commonly used in particle systems [25], as well as good convenience for managing

Table 1 Femur reconstruction errors for medio-lateral (X), antero-posterior (Y) and proximo-distal (Z) translations [mm], and for flexion/extension (α), abduction/adduction (β) and internal/external rotation (γ) [deg]

	X	Y	Z	α	β	γ
Mean	0.45	0.19	0.37	3.28	1.49	0.43
RMS	0.59	0.24	0.4	3.86	1.71	0.55
Std	0.4	0.16	0.17	2.06	0.89	0.37

collisions, contacts and other geometrical constraints efficiently.

This model has been optimized to the context of large deformations through the corotational scheme: this avoids the nonlinearity of shear deformations by expressing the deformation state of the material in a local coordinate system oriented along the eigendirections of the strain tensor [27, 42]. This preserves accuracy in the linearized expression of the material strain, allowing linearity to offer a more robust processing of high compression states than the Saint-Venant–Kirchhoff models usually implemented in the context of large deformations [7, 26, 44].

We have associated this model to an adapted numerical integration scheme which uses either Newton–Raphson or Backward Euler steps, depending if static relaxation or dynamic simulation is used. Both take advantage of an efficient implementation of the Conjugate Gradient method which allows variable force Jacobian matrices to be accurately taken into account, key to an accurate processing of the nonlinearities resulting from large deformations.

This system provides us with a good performance in computing the strain and stress states of the deformable tissues, which can then be rendered interactively though adequate visualization techniques.

4 Results

4.1 Morphological analysis

Since our goal is to investigate idiopathic OA, we must first eliminate the typical abnormalities of the hip joint that could lead to cam/pincer FAI. Therefore, a morphological analysis is performed to evaluate the prevalence of the subject's hip joint. The morphology of the hip is well described by selected anatomical parameters.

One important parameter is the computation of the acetabular version which can be an indicator of pincer FAI [43]. We have implemented the standard measurement method from [45]. It is based on the angle between the sagittal direction and lines drawn between the anterior and posterior acetabular rim, at different heights (Fig. 5a). The angle is considered as positive when inclined medially to the sagittal plane (anteversion) and negative when inclined laterally to the sagittal plane (retroversion). Normal hips are anteverted.

Another indicator of pincer FAI is the acetabular depth [43]. The depth of the acetabulum is defined as the distance in mm between the center of the femoral head (O) and the line AR–PR connecting the anterior (AR) and posterior (PR) acetabular rim (Fig. 5b). The value is considered as positive and normal if O is lateral to the line AR–PR.

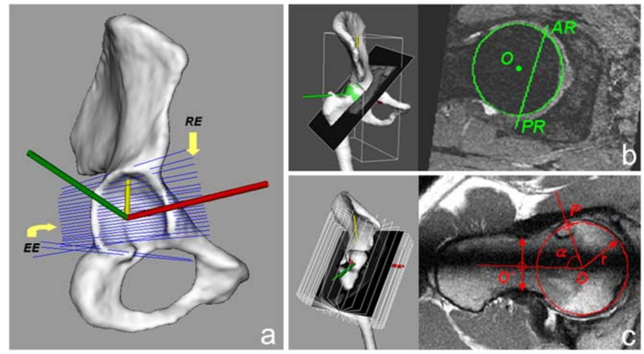

Fig. 5 (**a**) Computation of the acetabular version based on 3D reconstruction; roof edge (RE) and equatorial edge (EE) are lines drawn between the anterior and posterior acetabular edges, defining the orientation of the acetabular opening proximally and at the maximum diameter of the femoral head respectively (*arrows*). (**b**) Definition of the acetabular depth (*right*) on a transverse oblique MR image (*left*). (**c**) Definition of the α angle (*right*) on a radial MR image (*left*), illustrating a cam type morphology ($\alpha = 85°$)

Finally, a standard parameter related to the femur geometry is the femoral alpha (α) neck angle that is used for detecting cam FAI [43]. The α angle is being defined by the angle formed by the line O–O' connecting the center of the femoral head (O) and the center of the femoral neck (O') at its narrowest point, and the line O–P connecting O and the point P where the distance between the bony contour of the femoral head and O exceeds the radius (r) of the femoral head (Fig. 5c). Deviation from the normal geometry is usually associated with larger α angles (>60°).

All the dancers' hips were analyzed, according to those 3 anatomical parameters. No morphological abnormalities were detected and it was concluded that all the measured hips were anteverted, with a positive depth and an α angle in the normal range ($30° < \alpha < 55°$). The results were validated by a radiological expert.

4.2 Physical simulation

Simulation results are presented for one dancer. They were obtained during the simulation of the hip joint, where the labral deformations and pressures were computed. The elements present in our tests were: the hip and femur bones, as well as the tetrahedralized labrum. We investigated the three dancing's movements (grand plié, frontal split and developpé à la seconde) recorded from the motion capture, as motion input. Since they all require extreme hip flexion and/or abduction, they should create significant stress in the articulation.

All the biomechanical materials considered in the current study were assumed as linear elastic and isotropic. The 3D models of the bones were hypothesized as rigid bodies, and the material properties for the labrum in terms of elastic modulus (Young's modulus E) and Poisson's ratio (ν) were defined to be 20 MPa and 0.4, as depicted in [18].

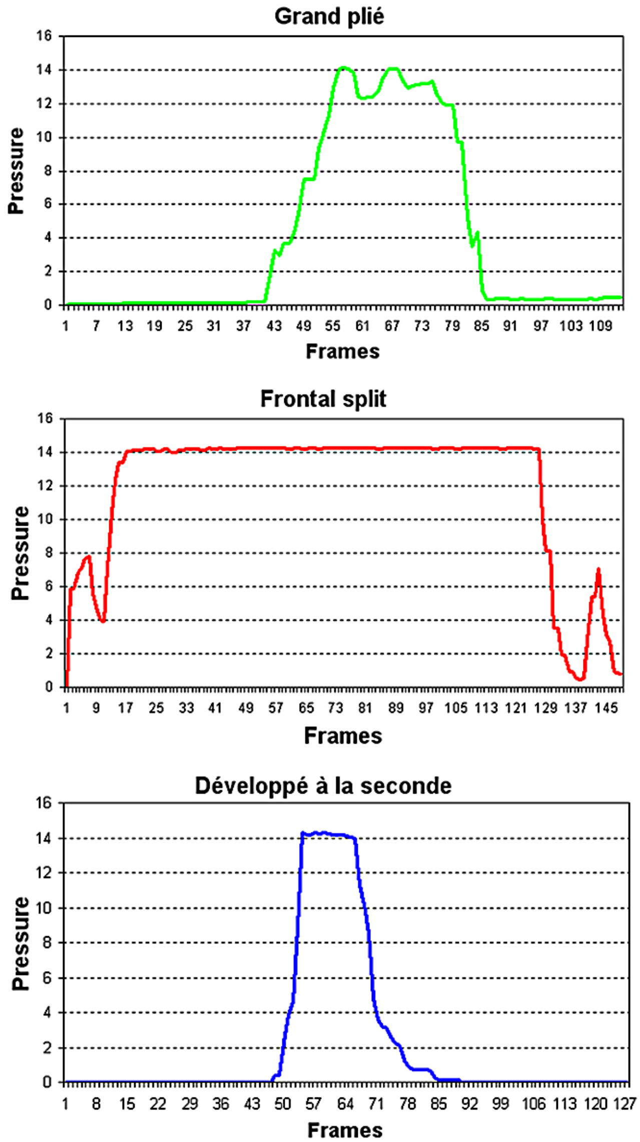

Fig. 6 Peak contact pressures of the labrum during the whole motion

The mechanical simulation first detects the collisions between the femur and labrum surfaces, using the previous approach described in Sect. 3.3. Then, an appropriate collision response is computed, based on quadratic penalty forces [28]. The aim is to constrain the two models to reach the non-penetrating state.

We define the pressure P as the stress along the direction of the maximal compression. For each movement, the peak contact pressures of the labrum are plotted, as a function of motion (Fig. 6). Furthermore, Fig. 7a shows for the three motions the pressure distribution within the labrum, for the instant frame where the maximal pressure was computed. Finally, Table 2 presents, for the three movements, the maximal and average peak pressures calculated during the entire motion, but only when collisions were detected.

Table 2 Maximal and average peak pressures within the labrum, calculated during the entire motion, but only when collisions were detected

Movement	Peak (MPa)	Mean (MPa)
Grand plié	14.12	10.18
Frontal split	14.28	11.95
Developpé à la seconde	14.27	9.16

4.3 Interpretation

The subject's MR images were analyzed by a radiological expert. For the tested dancer, the localization of the labral lesions were diagnosed for both hips in the superior region of the acetabular rim. The labrum was considered as degenerated (abnormal signal intensity) for the left hip and torn (abnormal linear intensity extending to the labral surface) for the right hip. According to the three anatomical parameters, the morphological analysis for this subject reported an α angle of 42.95° (left hip) and 43.67° (right hip), an acetabular depth of 8.06 mm (left hip) and 7.72 mm (right hip) and no retroversion. Thus, the subject's hips did not present any cam or pincer type morphology.

For the three movements analyzed, the maximal peak contact pressures occurred at maximal hip joint angle, as shown in Fig. 7a. Strong labral deformations were observed when the subject was performing extreme hip flexions or abductions. Moreover, the labral deformations were located in the superior area of the acetabular rim, which corresponds to the localization of diagnosed lesions (Fig. 7b). Finally, according to Table 2, the calculated maximal and average peak pressures are high compared to the normal situation. Indeed, previous studies [14, 46] reported cartilages pressures ranging from 2 MPa to 4 MPa for asymptomatic hips and daily activities. This corroborates the fact that the articulation undergoes a high stress during extreme hip motion. Moreover, Fig. 6 reveals that such high pressures are often reached during dancing activities.

In conclusion, the simulation clearly demonstrates that both the pressure and its distribution within the labrum are clinically relevant with respect to radiologically observed damage zones in the labrum.

5 Discussion

In this paper, a methodology to perform functional simulations of the hip joint in extreme postures has been described. The use of optical motion capture allows us to accurately estimate bone poses of patient-specific hip joint, whereas the physical simulation provides us with accurate labral deformations and pressure indications in the simulated joint.

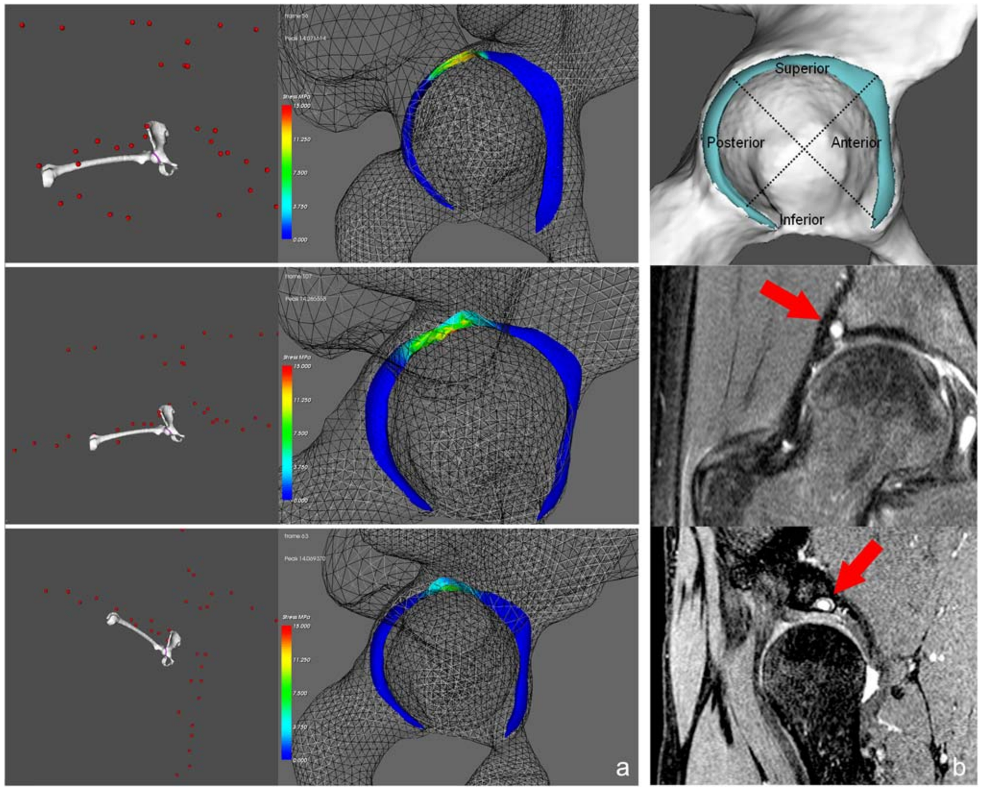

Fig. 7 (**a**) Computed motion and resulting pressure distribution within the labrum: grand plié (*top*), frontal split (*middle*) and developpé à la seconde (*bottom*). We clearly see that the maximal peak contact pressures occur at the maximal hip joint flexion and/or abduction. (**b**) *Top*: spatial partitioning of the acetabular region in quadrants. *Middle and bottom*: diagnosed labral lesions in patient's MR images (*red arrows*). The labral deformations (**a**) and the lesions (**b**) are both located in the superior quadrant of the acetabular rim

The simulation results have been reported for a single dancer, presenting no morphological abnormalities. These results already reveal that motion has a direct influence on the pressure distribution within the labrum. Moreover, a strong correlation is observed between the computed labral deformations and the diagnosed lesions. These are clinically encouraging results, but this methodology needs to be tested with additional subjects. However, there is little doubt that repetitive extreme hip motion could be a potential cause for the development of hip pain and OA in this selected population, with potential stigmata in the symptomatic dancers.

Future work will address the following points: The complex mechanical behavior of cartilage (i.e., nonlinear and biphasic properties) will be considered. A more advanced simulation accounting for all the cartilages of the hip joint (labrum, acetabular and femoral cartilages) will also be investigated. Finally, further experiments will be carried out to estimate the error made on the hip kinematics during extreme movements, since currently only low amplitude motion was validated. For example, these experiments can be conducted in open MRI.

Acknowledgements This work is supported by the Co-Me project funded by Swiss National Research Foundation and by the FOCUS K3D project (FP7-ICT-2007-214993) funded by the European Union. We would like to thank the University Hospital of Geneva, Professor Pierre Hoffmeyer, Dr. Jacques Menetrey and Dr. Frank Kolo-Christophe, Etienne Lyard, Marlène Arévalo and Nedjma Cadi for their collaboration. We are also grateful to all volunteers from the ballet of the Great Theater of Geneva to have accepted to take part in the study.

References

1. Ahmet, C., Vahdet, U., Recep, K.: Three-dimensional anatomic finite element modelling of hemi-arthroplasty of human hip joint. Trends Biomater. Artif. Organs **21**, 63–72 (2007)
2. Alexander, E., Andriacchi, T.: Correcting for deformation in skin-based marker systems. J. Biomech. **34**, 355–361 (2001)
3. Assassi, L., Guillard, G., Gilles, B., Magnenat-Thalmann, N.: Volumetric meshes based on medial representation for medical applications. In: Proc. Comput. Assist. Orthop. Surg. (CAOS'07), pp. 259–262 (2007)
4. Bathe, K.: Finite Element Procedures. Prentice-Hall, Englewood Cliffs (1995)
5. Benoit, D., Ramsey, D., Lamontagne, M., Xu, L., Wretenberg, P., Renstroem, P.: Effect of skin movement artifact on knee kinematics during gait and cutting motions measured in vivo. Gait Posture **24**(2), 152–164 (2006)
6. Binningsley, D.: Tear of the acetabular labrum in an elite athlete. Br. J. Sports Med. **37**, 84–88 (2003)
7. Bonet, J., Wood, R.: Nonlinear Continuum Mechanics for Finite Element Analysis. Cambridge University Press, Cambridge (1997)
8. Brown, T.: In vitro contact stress distributions in the natural human hip. J. Biomech. **16**, 373–384 (1983)
9. Cappello, A., Stagni, R., Fantozzi, S., Leardini, A.: Soft tissue artifact compensation in knee kinematics by double anatomical landmark calibration: Performance of a novel method during selected motor tasks. IEEE Trans. Biomed. Eng. **52**(2), 992–998 (2005)
10. Cappozzo, A., Catani, F., Croce, U.D., Leardini, A.: Position and orientation of bones during movement: anatomical frame definition and determination. Clin. Biomech. **10**, 171–178 (1995)
11. Cappozzo, A., Catani, F., Leardini, A., Benedetti, M., Croce, U.D.: Position and orientation in space of bones during movement: experimental artefacts. Clin. Biomech. **11**(2), 90–100 (1996)

12. Cereatti, A., Croce, U.D., Cappozzo, A.: Reconstruction of skeletal movement using skin markers: comparative assessment of bone pose estimators. J. NeuroEng. Rehabil. **3**(7) (2006)
13. Chegini, S., Beck, M., Ferguson, S.: The effects of impingement and dysplasia on stress distributions in the hip joint during sitting and walking: a finite element analysis. J. Orthop. Res. **27**(2), 195–201 (2008)
14. Chegini, S., Beck, M., Fergusson, S.: Femoro acetabular impingement as a possible initiator of cartilage degeneration. In: 7th Int. Symp. on Comput. Meth. in Biomech. and Biomed. Eng. (CMBBE2006), pp. 705–710 (2006)
15. Cotin, S., Delingette, H., Ayache, N.: Real-time elastic deformations of soft tissues for surgery simulation. IEEE Trans. Vis. Comput. Graph. **5**(1), 62–73 (1999)
16. Croce, U.D., Leardini, A., Chiari, L., Cappozzo, A.: Human movement analysis using stereophotogrammetry. Part 4: Assessment of anatomical landmark misplacement and its effects on joint kinematics. Gait Posture **21**, 226–237 (2005)
17. Dy, C., Thompson, M., Crawford, M., Alexander, J., McCarthy, J., Noble, P.: Tensile strain in the anterior part of the acetabular labrum during provocative maneuvering of the normal hip. J. Bone Joint Surg. Am. **90**, 1464–1472 (2008)
18. Ferguson, S., Bryant, J., Ito, K.: The material properties of the bovine acetabular labrum. J. Orthop. Res. **19**, 887–896 (2001)
19. Ganz, R., Parvizi, J., Beck, M., Leunig, M., Notzli, H., Siebenrock, K.: Femoroacetabular impingement: a cause for osteoarthritis of the hip. Clin. Orthop. Relat. Res. **417**, 112–120 (2003)
20. Garling, E., Kaptein, B., Mertens, B., Barendregt, W., Veeger, H., Nelissen, R., Valstar, E.: Soft-tissue artefact assessment during step-up using fluoroscopy and skin-mounted markers. J. Biomech. **40**, 18–24 (2007)
21. Gilles, B.: Anatomical and kinematical modelling of the musculoskeletal system from MRI. Ph.D. thesis, Université de Genève (2007)
22. Gilles, B., Moccozet, L., Magnenat-Thalmann, N.: Anatomical modelling of the musculoskeletal system from MRI. In: Med. Image Comput. Comp. Assist. Intervention (MICCAI'06), pp. 289–296 (2006)
23. Gilles, B., Perrin, R., Magnenat-Thalmann, N., Vallée, J.P.: Bones motion analysis from dynamic MRI: acquisition and tracking. Acad. Radiol. **12**, 2385–2392 (2005)
24. Gottschalk, S., Lin, M., Manocha, D.: Obbtree: A hierarchical structure for rapid interference detection. In: SIGGRAPH'96, pp. 171–180 (1996)
25. Hauth, M., Etzmuss, O.: A high performance solver for the animation of deformable objects using advanced numerical methods. In: Eurographics'01, pp. 137–151 (2001)
26. Hauth, M., Gross, J., Strasser, W.: Interactive physically-based solid dynamics. In: Eurographics Symp. Comput. Animation, pp. 17–27 (2003)
27. Hauth, M., Strasser, W.: Corotational simulation of deformable solids. In: WSCG'04, pp. 137–145 (2004)
28. Hirota, G., Fisher, S., State, A., Lee, C., Fuchs, H.: An implicit finite element method for elastic solids in contact. In: Comput. Animation, pp. 136–146 (2001)
29. Hodge, W., Carlson, K., Fijan, R., Burgess, R., Riley, P., Harris, W., Mann, R.: Contact pressures from an instrumented hip endoprostheses. J. Bone Joint Surg. Am. **71A**, 1378–1386 (1989)
30. Holden, J., Orsini, J., Siegel, K., Kepple, T., Gerber, L., Stanhope, S.: Surface movement errors in shank kinematics and knee kinetics during gait. Gait Posture **5**, 217–227 (1997)
31. Kepple, T., Arnold, A., Stanhope, S., Siegel, K.: Assessment of a method to estimate muscle attachments from surface landmarks: a 3d computer graphics approach. J. Biomech. **27**, 365–371 (1994)
32. Kumagai, M., Kim, Y., Inoue, N., Genda, E., Liong, K.H.B., Koo, T., Chao, E.: 3-D dynamic hip contact pressure distribution in daily activities. In: Summer Bioeng. Conf., pp. 53–54 (2003)
33. Lafortune, M., Cavanagh, P., Sommer, H., Kalenak, A.: Three-dimensional kinematics of the human knee during walking. J. Biomech. **25**(4), 347–357 (1992)
34. Lawrence, C., Tits, A.: A computationally efficient feasible sequential quadratic programming algorithm. SIAM J. Optim. **11**(4), 1092–1118 (2001)
35. Lewis, C., Sahrmann, S.: Acetabular labral tears. Phys. Ther. **86**, 110–121 (2006)
36. Lu, T., O'Connor, J.: Bone position estimation from skin marker co-ordinates using global optimisation with joint constraints. J. Biomech. **32**, 129–134 (1999)
37. Lucchetti, L., Cappozzo, A., Cappello, A., Croce, U.D.: Skin movement artefact assessment and compensation in the estimation of knee joint kinematics. J. Biomech. **31**(11), 977–984 (1998)
38. Maciel, A., Sarni, S., Boulic, R., Thalmann, D.: Stress distribution visualization on pre- and post-operative virtual hip joint. In: Proc. Comp. Assist Orthop. Surg. (CAOS'05), pp. 298–301 (2005)
39. Manal, K., McClay, I., Richards, J., Galinat, B., Stanhope, S.: Knee moment profiles during walking: errors due to soft tissue movement of the shank and the influence of the reference coordinate system. Gait Posture **15**, 10–17 (2002)
40. Mason, J.: Acetabular labral tears in the athlete. Clin. Sports Med. **20**, 779–790 (2001)
41. Mavcic, B., Pompe, B., Antolic, V., Daniel, M., Iglic, A., Kralj-Iglic, V.: Mathematical estimation of stress distribution in normal and dysplastic human hips. J. Orthop. Res. **20**, 1025–1030 (2002)
42. Nesme, M., Payan, Y., Faure, F.: Efficient, physically plausible finite elements. In: Eurographics'05, pp. 77–80 (2005)
43. Pfirrmann, C.W.A., Mengiardi, B., Dora, C., Kalberer, F., Zanetti, M., Hodler, J.: Cam and pincer femoroacetabular impingement: Characteristic mr arthrographic findings in 50 patients. J. Radiol. **240**(3), 778–785 (2006)
44. Picinbono, G., Delingette, H., Ayache, N.: Non-linear anisotropic elasticity for real-time surgery simulation. Graph. Model. **65**(5), 305–321 (2003)
45. Reynolds, D., Lucas, J., Klaue, K.: Retroversion of the acetabulum, a cause of hip pain. J. Bone Joint Surg. **81**(2), 281–288 (1999)
46. Russell, M., Shivanna, K., Grosland, N., Pedersen, D.: Cartilage contact pressure elevations in dysplastic hips: a chronic overload model. J. Orthop. Surg. Res. **1**(6), 169–177 (2006)
47. Schneider, P., Eberly, D.: Geometric Tools for Computer Graphics. The Morgan Kaufmann Series in Computer Graphics and Geometric Modeling (2003)
48. Seo, H., Magnenat-Thalmann, N.: An automatic modeling of human bodies from sizing parameters. In: ACM SIGGRAPH 2003 Symp. on Interact. 3D Graph, pp. 19–26 (2003)
49. Söderkvist, I., Biomech, P.W.J.: Determining the movements of the skeleton using well-configured markers. J. Biomech. **12**, 1473–1477 (1993)
50. Stagni, R., Fantozzi, S., Cappello, A., Leardini, A.: Quantification of soft tissue artifact in motion analysis by combining 3d fluoroscopy and stereophotogrammetry: a study on two subjects. Clin. Biomech. **20**, 320–329 (2005)
51. Wu, G., Siegler, S., Allard, P., Kirtley, C., Leardini, A., Rosenbaum, D., Whittle, M., D'Lima, D., Cristofolini, L., Witte, H., Schmid, O., Strokes, I.: ISB recommendation on definitions of joint coordinate system of various joints for the reporting of human joint motion—part I: Ankle, hip and spine. J. Biomech. **35**(4), 543–548 (2002)

Caecilia Charbonnier is an Engineer in Computer Science. She obtained her Master of Advanced Studies degree in 2006 in Computer Graphics at the EPFL (Federal Polytechnic school of Lausanne), Switzerland. She is currently a Ph.D. candidate and research assistant at MIRALab, working in medical simulation. Her interests include motion analysis, ontology, segmentation, surface deformation, optimization algorithms and multi-modal acquisition techniques (Mocap, 3D body scanner, EMG, etc.).

Lazhari Assassi is Engineer in Electronics. He obtained his Master degree in Electronics in 1996 at Setif University, Algeria. Until 2003, he was Assistant Professor at Biskra University, Algeria. In 2005, he received his Master degree in Information and Communication Systems (Visualization and Graphics Communication) at University of Geneva, Switzerland. Currently, he is a Ph.D. candidate and research assistant at MIRALab, working in medical informatics. His interests include volumetric modeling, deformable models and physically-based simulation.

Pascal Volino finished his Ph.D. thesis in 1998 at the University of Geneva, Switzerland. He is a computer scientist, working at MIRALab, University of Geneva. He is actually working on new models for cloth animation, involving versatile models for efficient simulations on situations involving high deformation, wrinkling and multilayer garments. The research is particularly focused on robust simulation and interactive cloth manipulation. His work is taking part of the several EU projects, involving creation and simulation of virtual garments.

Nadia Magnenat-Thalmann has pioneered research into Virtual Humans over the last 25 years. She obtained several Bachelor's and Master's degrees in various disciplines (Psychology, Biology and Chemistry) and a Ph.D. in Quantum Physics from the University of Geneva. From 1977 to 1988, she was a Professor at the University of Montreal in Canada where she founded the research lab MIRALab. She moved to the University of Geneva in 1989 and recreated the Swiss MIRALab, an internationally interdisciplinary lab. She is the coordinator of different European and National Swiss research projects, among them on medical topics 3D ANATOMICAL HUMAN, CO-ME and CHARM. She is Editor-in-Chief of the Visual Computer Journal published by Springer Verlag and associate editor of IEEE Transactions on Multimedia.